POLITECNICO DI TORINO
Repository ISTITUZIONALE

Conditional generative adversarial networks for the data generation and seismic analysis of above and underground infrastructures

(Article begins on next page)

09 January 2025

Conditional generative adversarial networks for the data generation and seismic analysis of above and underground infrastructures

M. Dalmasso [ID], M. Civera [*][ID], V. De Biagi , C. Surace [ID], B. Chiaia

Department of Structural, Building and Geotechnical Engineering, Politecnico di Torino, Torino, Italy

ARTICLE INFO

ABSTRACT

Estimating the resilience of civil infrastructures is crucial for disaster prevention (i.e. earthquakes), encompassing both above- and underground constructions. However, while below-ground infrastructures are generally acknowledged as less vulnerable than their over-ground counterparts, this aspect has not yet garnered widespread attention. Thus, noting the limited number of seismic response comparisons for underground structures and the virtual absence of comparative analysis between above- and below-ground infrastructures in the scientific literature, this work aims to address this research gap. Nevertheless, data scarcity strongly hampers this endeavour. Not only do very few tunnels have permanent dynamic monitoring systems installed, but even fewer recorded major earthquakes are in proximity to similarly instrumented bridges and viaducts. This study focuses on three infrastructures of the San Francisco Bay Area: the Bay Bridge, the Caldecott Tunnel and the Transbay Tube. The chosen infrastructures represent a unique combination of nearby, continuously monitored case studies in a seismic zone. Yet, even for these selected infrastructures, few comparable data are available – e.g., only one earthquake was recorded for all three. Hence, a Conditional Generative Adversarial Network (CGAN) technique is put forward as a strategy to build a hybrid dataset, thereby incrementing the available data and overcoming the data scarcity issue. The CGAN can generate new data that resemble the real ones while simultaneously comparing different datasets via binary classification. With this dual objective in mind, the CGAN algorithm has been applied to various cases, varying the input given in terms of selected acquisition channels, infrastructure pairs, and selected strong motions. In conclusion, each pair underwent a postprocessing phase to analyse the results. This research's outcomes show that the classifications performed with the Support Vector Machine reached excellent results, with an average of 91.6% accuracy, 93.1% precision, 93.3% recall, and 92.9% F1 score. The comparison in the time and frequency domain confirms the resemblance.

1. Introduction

Structural Health Monitoring (SHM) is one of the most important topics in civil engineering, especially since several buildings and infrastructures are approaching or surpassing the end of their service life. Additionally, the ever-increasing traffic loads and variations due to climate change exacerbate the situation. For these reasons, it is critical to have a dynamic monitoring system that can define the conditions of the infrastructures from its vibrational response. Such systems are especially important whenever earthquakes impact the monitored infrastructure. However, to properly deploy and operate such SHM apparatuses, it is necessary to clearly understand the expected dynamic response; this has not yet been totally defined for underground systems,

mainly due to a lack of experimental data.

Indeed, several examples in the literature describe the seismic behaviour of bridges – (He et al., 2022; Jiang et al., 2020; Mccallen et al., 2005) – while few works have analysed the behaviour of tunnels. Some noteworthy examples include (Bana e Costa et al., 2008; Bilotta et al., 2014; Dikmen, 2016; G. Lanzano et al., n.d.). The authors (Tsinidis et al., 2020) recently presented a very comprehensive state-of-the-art review on the seismic response and design of tunnels. Similarly, (Lanzano et al., 2012) provided an experimental benchmark on the seismic behaviour of tunnels in sand.

However, the topic deserves further attention. As evidenced by well-established sources (Chen et al., 2012), the pertinent literature indicates that earthquakes can potentially damage tunnels. Noteworthy instances
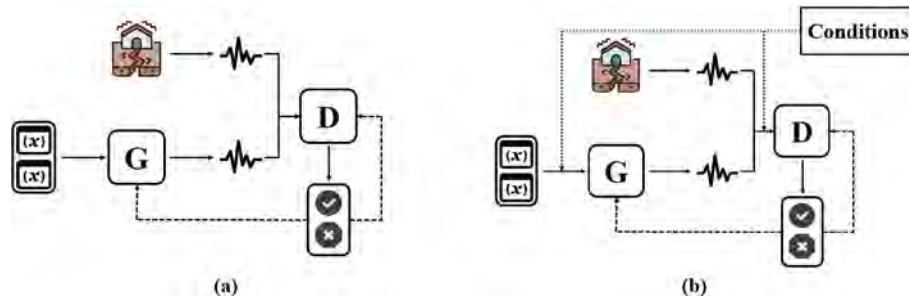

Fig. 1. Schematization of the operation of the GAN in **(a)** and CGAN **(b)**.

of seismic tunnel damage have been documented in Japan from 1923 to 2007. Specifically, there were 82 reported instances associated with the 1923 Kanto earthquake (Okamoto S., 1984), 20 cases linked to the 1995 Kobe earthquake (Asakura & Y. Sato, 1998), over 50 instances related to the 2005 Niigataken-Chuetu earthquake (Chen et al., 2012), and six instances tied to the 2007 Niigataken Chuetu-Oki earthquake. In Taiwan, the 1935 Hsinchu-Taichung earthquake caused damage to the old Sanyi railway tunnels, and the very well-known 1999 Chi-Chi earthquake led to damage in 49 tunnels (Hwang & Lu, 2007; Wang et al., 2001). Seismic tunnel damage has also been reported in other countries, including the USA and elsewhere (Tsinidis et al., 2016). Global databases documenting seismic damage to tunnels exist. For instance, (Charles H. Dowding & Arnon Rozan, 1978) compiled 71 cases of seismic damage to tunnels, while (Sharma & Judd, 1991) grouped 192 instances of damage to underground structures across 85 countries. These records highlight the need to investigate seismic damage to tunnels.

In this regard, the authors' initial aim was solely to directly compare the behaviour of infrastructure above and underground (specifically, nearby bridges and tunnels) under the same seismic excitation. The data originates from the database of the Center for Engineering Strong Motion Data (CESMD) (Haddadi et al., n.d.). More specifically, this work is based on the records of transversal sensors coming from the monitoring system applied on the Bay Bridge (BB), the Transbay Tube (TT) and the Caldecott Tunnel (CT), which are important infrastructures located in the San Francisco Bay Area, California, USA. Each infrastructure is equipped with a dynamic monitoring system, triggered during major seismic events.

Due to a lack of available experimental datasets in this and other well-acknowledged strong motion repositories, it was decided to focus on data generation techniques, which became the core of this research study. Data generation approaches allow the creation of synthetic datasets statistically compatible with the one given in input (the actual measured data). Data generation should not be confused with data augmentation, which consists of enhancing the size of the data by copying the existing data and applying the transformation by means of adjustments to increase the diversity and the amount of data in the dataset. Thus, this paper's main aim is the creation of hybrid datasets made of experimental and realistic, numerically generated strong motion records and the successive analysis to assess the resemblance of generated data with the original data.

For this main aim, it was decided to adopt a Machine Learning (ML) approach, in particular, Generative Adversarial Networks (GAN). This was inspired by the several applications of GAN in the SHM field published in the last few years (Luleci et al., 2022) and motivated by the need to provide statistically reliable generated data.

The peculiarity of the intended goal led to the use of a particular type of GAN, the Conditional Generative Adversarial Network (CGAN). The CGAN is an evolution of the better-known GAN; more specifically, its application is to generate data that resemble (from a statistical perspective) the real ones, as for the standard GAN, but that belong to different classes (in this case, different infrastructures). This further

allows not only to generate new data but also, at the same time, to compare the various behaviours of the two classes (i.e., for instance, above- and below-ground infrastructures, or different underground infrastructures).

The remainder of this paper is organised as follows. In Section 2, the proposed algorithm for data generation and data comparison is introduced and described in its implementation. In Section 3, the case studies are briefly introduced, along with the criteria used for their selection. Section 4 further details the case analysed in terms of selected seismic events, recordings, and pairwise comparisons. The Results are presented and discussed in Section 5 and the Conclusions (Section 6) conclude this paper.

2. GAN, CGAN, and binary classification algorithm

The concept of GAN was introduced by (Goodfellow et al., 2014). It is a deep learning technique that can produce new, plausible samples based on the input data it receives.

Goodfellow and his team illustrated the operation of GAN with the following example: "*The generative model can be thought of as analogous to a team of counterfeiters, trying to produce fake currency and use it without detection, while the discriminative model is analogous to the police, trying to detect the counterfeit currency. Competition in this game drives both teams to improve their methods until the counterfeits are indistinguishable from the genuine articles*" (Goodfellow et al., 2014).

GAN is an adversarial process that concurrently trains two models: the Generative model (G) and the Discriminative model (D). The duty of the Generative model (also called the Generator) is to comprehend the data distribution and to generate data starting from random values. The relative training procedure aims to maximise the probability of the discriminative model making a mistake. The Discriminative model (also called Discriminator) assesses the probability that a given sample originates from the training set or the G. The training of the D aims to distinguish between the real and the generated data. As the two models are pitted against each other as an adversary, the competition carries both models to enhance their performances. Thus, in GAN modelling, both the G and D during training are in constant competition. While G tries to 'fool' and confuse the discriminator by generating increasingly realistic data, D strives to differentiate between authentic data from the fake data generated by G (Sarker, 2021).

A schematic representation of the GAN functioning is depicted in Fig. 1 (a). The formal description of the process details can be found in (Goodfellow et al., 2014) and subsequent works from the same authors (Salimans et al., n.d.; Fedus et al., 2017).

A limitation in the use of the GAN is the capability of this network to work with only one label. This is a remarkable limitation of the basic GAN approach since it does not allow the comparison of the seismic responses of different infrastructures. This issue was solved by adopting the CGAN. The CGAN can use labelled data in the training phase to create data that belong to definite categories. A CGAN can be implemented by adding a supplementary conditional model to both G and D. The condition is fed into D and G could be of different types, such as class
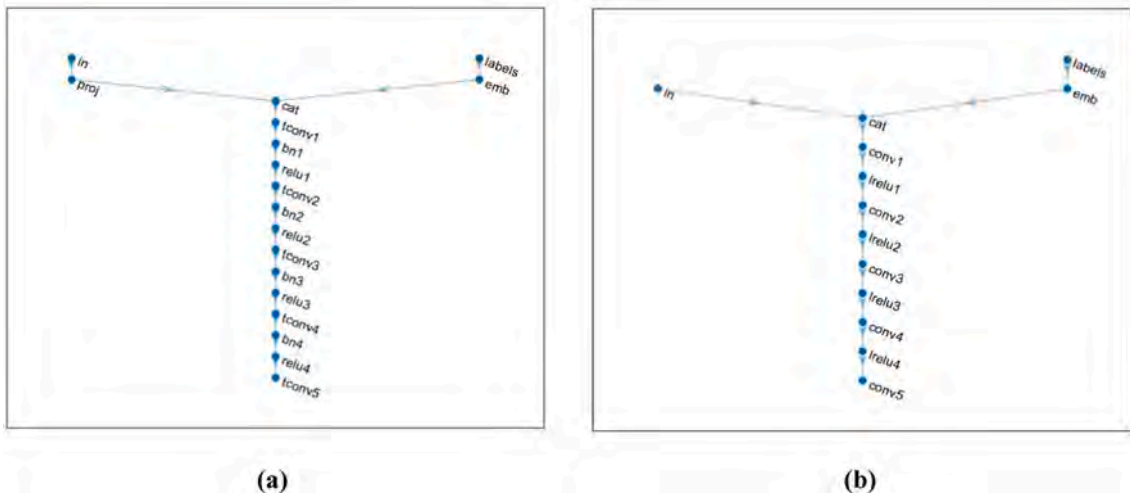
Fig. 2. Architectures of G **(a)** and D **(b)**. in:input layer; proj: project and reshape layer; labels: label layer; emb: embedding and reshape layer; cat: concatenation layer; tconv: transposed convolutional 2D layer; bn: batch normalization layer; relu: ReLu layer; lrelu; leaky ReLu layer.

labels or data from other methods (Mirza & Osindero, 2014). A schematic representation of the CGAN functioning is depicted in Fig. 1 (b).

For this application, the algorithm is built to deal with 1D problems and two classes. The problem's dimensionality derives from the intention to use the recorded acceleration time series, taking each sensor channel separately. The algorithm is built on Matlab™ R2022a, an environment for numerical calculation and statistical analysis, augmented with the *'Signal Processing Toolbox'*, *'Statistics and Machine Learning Toolbox'* and *'Deep Learning Toolbox'*.

Once the input data are given, the code comprises several sections that allow the definition of G and D, train them, and generate realistic data. Furthermore, the conventional CGAN procedure is expanded to include a binary classification as a next step to discern between two classes. These stages are described in the following step-by-step list. To make the process easier to follow, the list refers to the specific sizes used in this particular application; nevertheless, the procedure can be generalised to different datasets.

- **Pre-processing and loading the training data**: to make all the analyses comparable, it was decided to use the same size and number of training data for all datasets. Specifically, 1575 vector columns, each composed of 1201 elements (or data points), were used to accommodate a substantial dataset of time series. Each time series is long enough to encompass the vibrations induced by the earthquake. As mentioned, these arrays correspond to acceleration time series with a constant time step between the elements. The fixed length accommodates the recorded acceleration vectors composed of a variable number of elements, different for each seismic event and station. Furthermore, since most records comprise pre- and post-event ambient vibrations, it was decided to truncate the signals, focusing on the most significant part after the initial shock. Thus, only the timesteps representing the oscillation caused by the strong motion have been used for each recorded channel. Furthermore, as it is good practice in ML approaches (Farrar & Worden, 2012), the training dataset is normalised employing z-score standardisation; i. e., the mean value is subtracted from the array elements, and the result is divided by their standard deviation. The resulting arrays have zero mean and unit variance and are, thus, statistically comparable.
- **Defining the architecture of the Generator Network**: G starts from a matrix of random values. In the most general case, this is a multi-dimensional tensor (to accommodate 1D or 2D data) and a given number of latent inputs. In this specific case, 100 latent inputs are set, following a common default value and thus resulting in a tensor

with size $1 \times 1 \times 100$. These represent the initial Gaussian distribution at the beginning of the training phase. Then, the Generator network has to:

- o Project and reshape the initial tensor of random values to transform them into the desired sizes (here, $4 \times 1 \times 1024$). The custom layer achieves this by upscaling the input through a fully connected layer and then reshaping the resulting output to meet the desired dimensions;
- o Provide the labels into the network, considering the four possibilities available in a binary classification case: real data case 1, real data case 2, generated data case 1, generated data case 2;
- o Convert the labels into embedding vectors and reshape them (in this case, to a $4 \times 1 \times 1$ tensor). Another custom layer is utilised to perform this operation. This layer converts categorical labels into one-channel arrays of the specified size through embedding and fully connected operations;
- o Concatenate the random values and the labels, appending these latter ones and thus reaching, in this particular case, a $4 \times 1 \times 1025$ tensor;
- o Upsample the resulting arrays to match the input data size (as mentioned, $1201 \times 1 \times 1$ here), adopting a sequence of 1-D transposed convolution layers that incorporate batch normalisation and ReLU layers.
- **Defining the architecture of the Discriminator Network:** D classifies the authentic and the generated 1D signals given the input data set and the corresponding labels. The (real or generated) 1201×1 time series are taken as input. Then, the D has to:
- o Convert the categorical labels into an embedding vector and then reshape them into a $1201 \times 1 \times 1$ tensor;
- o Concatenate the results from the two inputs along the channel dimension, resulting in an output that has a size of $1201 \times 1 \times 1025$;
- o Downsample the resulting tensor to a scalar prediction score (i.e. a $1 \times 1 \times 1$ value). This is achieved by adopting a sequence of 1-D convolution layers with leaky ReLU layers.

In Fig. 2, the architectures of G and D are depicted, with all the hidden layers adopted.

- **Training the two adversarial models**: the training is accomplished using a custom training loop. This iterates over the training data and refreshes the network parameters at every cycle. Also, for each epoch, the training data are randomised (via a classic shuffling procedure) and iterated through data mini-batches.

- **Synthesising the generated signals**: the generation process is performed in the generator network on a batch of $1 \times 1 \times 100$ tensors, initialised with random values. Arbitrarily, it was chosen to generate 2000 samples, where the first 1000 samples correspond to label #1 and the remaining label #2. Notably, at this step, the standardisation process applied at the beginning is reversed, such that the generated time series are expressed with the same mean and standard deviation of the population of measured data from which they originated.

At this point, the CGAN training is complete. The post-processing phase follows this, which includes a visual comparison of the generated dataset, to verify the similarity with the real one, and then a binary classification process, based on Support Vector Machine (SVM) binary classification. The SVM, introduced in (Cortes & Vapnik, 1995), is a kernel ML model known for its exceptional generalisation ability, optimal solutions, and strong discriminative power. SVM showed excellent performance in classification, regression and forecasting. The core concept of SVM is mapping non-linear vectors into a very high-dimension feature space, where a linear decision surface (hyperplane) is constructed. The hyperplane is optimised as a maximal margin classier (Cervantes et al., 2020; Huibing Wang et al., 2017). This last step blindly labels the measured data after having been trained only on the generated data. This is intended to highlight the differences in the responses of the different infrastructures, which are learned and used by G to provide distinct generated data for the distinct tunnels or bridges.

- **Signal feature visualisation via PCA:** since the direct visual comparison of measured and generated signals is difficult (or almost impossible) directly in the time domain, it is better to perform such comparison after the application of the principal component analysis (PCA) (Wold et al., 1987). That way, a subset of the principal components can be used to build a more informative subspace, where the features of both the generated and the real signals can be projected and better investigated.

- **SVM training on generated data and validation through prediction on real data**: in this phase, the generated signals are used to train an SVM classifier and the recorded data are used as the test dataset. Particularly, here, SVMs utilise a polynomial kernel that can combine the features of the sample to determine the similarities, using a polynomial of order two and automated kernel scaling (see the Matlab guide[1] for further technical details). As shown in the Results, the correspondent accuracy, precision, and recall are reported together with a confusion matrix to view the prediction performed by the SVM classifier in detail.

- **Plot of the measured and generated data in the time and frequency domain**: the last step concerns the plot of the real (i.e. measured) acceleration time series versus the ones generated from the algorithm. The comparison is represented both in the frequency domain and in the time domain.

3. Description of the case studies

The infrastructures studied are located in the San Francisco Bay Area and instrumented with a monitoring system.

This selection was made after careful evaluation by the authors. The rationale was to find a group of infrastructures that fit the following requirements:

1. Include over- and below-ground infrastructures close to each other;
2. Include underground infrastructures of different kinds and boundary conditions;
3. Include as many parallel tracts as possible to ensure similar readings from sensor channels oriented similarly;
4. Being placed in a seismically active zone;
5. Include at least one seismic event shared among all infrastructures (and potentially other events shared among pairs of them).

The aforementioned BB, TT, and CT systems represent, to the best of the Authors' knowledge, the only publicly available datasets worldwide to fulfil these requirements.

The following subsections give a brief description of the aforementioned structures, presenting their structural characteristics and the geological context in which they are included. The last subsection describes the main features of the earthquakes considered.

3.1. Bay Bridge

The BB was constructed between 1933 and 1936 and spans the San Francisco Bay Area. Initially, the bridge comprised two structural typologies for two sections, divided by the presence of the Yerba Buena Island. After the Loma Pietra Earthquake, which happened on October 17, 1989, with a magnitude of $M_w = 6.9$, a retrofitting intervention was necessary for a new superstructure for the East part.

The West part was and still is a suspension bridge. The new (after Loma Pietra) East section, in turn, consists of several parts: the Yerba Buena Island transition structure, the self-anchored suspension bridge, the Skyway, and the Oakland touchdown.

In this work, the station corresponding to the Skyway (CE58601 in the CESMD inventory) was chosen, as this section runs almost parallel to the TT. This seismic station was installed during the retrofitting intervention and equipped with 73 sensors. These are positioned on the pile foundations, at the base, along the pier, and on the deck. They monitor the acceleration exhibited by the structure in three directions: longitudinal, transversal relative to the axis of the infrastructure, and vertical.

This interest portion is 2085 m long and divided into 13 spans with a nominal length of 160 m. The superstructure is a precast concrete box girder composed of two webs. The substructure comprises frame units consisting of three or four piers per frame, whilst the foundations are moment-resisting steel frames tied with cast-in steel shell concrete piles of diameter 2.5 m. The geological conditions of this tract of the Bay Bridge are the same as the ones that will be discussed in the following subsection for TT (Ho, n.d.; Nader et al., n.d.; The Loma Prieta, California, Earthquake of October 17, 1989, Highway Systems, n.d.).

3.2. Transbay Tube

The TT, also known as the Bay Area Rapid Transit (BART), is a submerged railroad tunnel in the San Francisco Bay. It links San Francisco with Oakland from 1974 when it opened. It develops side-by-side with the above-mentioned BB, running almost parallel to it in the tract of the Skyway.

From a geological and geotechnical perspective, the San Francisco Bay Area is composed of a stratum of Young Bay Mud (YBM), a normally consolidated organic marine clay with very low shear strength and prone to squeezing, and Old Bay Clay (OBC) over-consolidated clay. On the East flank of the Bay, there is a transition to alluvial sands with clay (Matteo Dalmasso et al., 2024).

The TT is 5.8 km long; at the extremities, it is linked to two boring tunnels that connect the TT to the rest of the network. The maximum depth of the tunnel relative to sea levels is -41 m. The TT was built adopting the immersion tube technique, where a trench of 18 m wide was excavated. Shortly afterwards, tubular steel and reinforced concrete segments were immersed and covered with gravel sand and rock. The typical cross-section comprises two parallel train tunnel bores divided by a pedestrian gallery used for emergencies. In the 2000s, the retrofitting led to interventions that limited the tube movement and the eventual gravel or sand liquefaction, employing compaction and the use

---

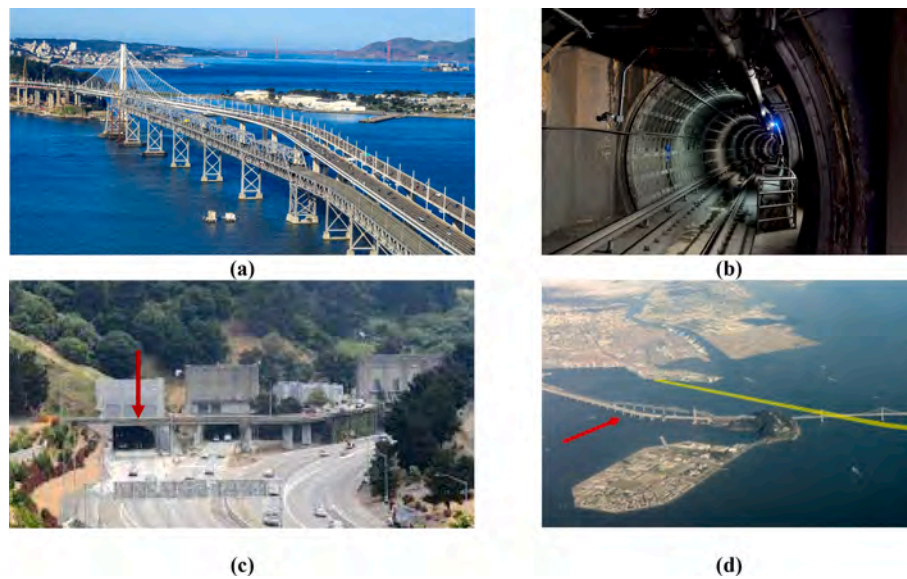[1] https://it.mathworks.com/help/stats/fitcsvm.html#bt9w6j6_sep_shared-KernelScale.

Fig. 3. The infrastructures studied here: **(a)** the BB, **(b)** the TT, and **(c)** the CT, where the arrow points to Bore 4. **(d)** compares the approximate route of TT, highlighted in yellow, and the BB tract of interest (the Skyway), almost parallel in its easternmost tract. The arrow indicates the instrumented Pier E6E along the Skyway. (For interpretation of the references to colour in this figure legend, the reader is referred to the web version of this article.)

Table 1
Numbering adopted in this work.

Bay Bridge (BB)		Transbay Tube (TT)		Caldecott Tunnel (CT)	
CESMD numbering	New numbering	CESMD numbering	New numbering	CESMD numbering	New numbering
Please refer to Figures A1 and A2 for a graphical illustration.		Please refer to Fig. A3 for a graphical illustration.		Please refer to Fig. A4 for a graphical illustration.	
28	BB-1	2	TT-1	1	CT-1
31	BB-2	8	TT-2	4	CT-2
34	BB-3	13	TT-3	7	CT3
42	BB-4	16	TT-4	10	CT-4
43	BB-5	19	TT-5	13	CT-5
44	BB-6	22	TT-6		
45	BB-7	25	TT-7		
48	BB-8	28	TT-8		
51	BB-9	31	TT-9		
56	BB-10	34	TT-10		
62	BB-11	39	TT-11		
65	BB-12				
68	BB-13				
73	BB-14				

Table 2
Summary of the characteristics of the six analyses.

Analyses:	Channels considered:	Earthquake considered:
I	**BB**: BB-4,5,6,7,8,9,10,11,12,13,14 **TT**: All channels (TT-1,2,3,4,5,6,7,8,9,10,11)	BE18
II	**BB:** All channels (BB-1 to BB-14) **TT**: All channels	BE18
III	**BB**: BB-4,5,6,7,8,9,10,11,12,13,14 **CT**: All channels (CT-1,2,3,4,5)	BE18
IV	**BB:** All channels **CT**: All channels	BE18
V	**TT**: All channels **CT**: All channels	BE18
VI	**BB**: BB-4,5,6,7,8,9,10,11,12,13,14 **TT**: All channels	**BB:** BE18 + SN14 + PE15 **TT**: BE18

of concrete encase supports (Michael Cabanatuan, 2004).

For Structural Health Monitoring purposes, the TT was instrumented with 40 sensors throughout its development, constituting the station called CE58580.

3.3. Caldecott tunnel

The CT is a deep tunnel that crosses the Berkeley Hills between Oakland and Orinda in a region geologically characterised by marine and non-marine sedimentary rocks such as sandstone and claystone. Additionally, the tunnel intersects four major inactive faults, perpendicularly to the tunnel alignment (Thapa et al., n.d.).

The infrastructure comprises four bores, built at different points in time to accommodate the ever-increasing road traffic between the San Francisco Bay Area and Central California. More specifically, Bores 1 and 2 were opened at the inauguration in 1937, Bore 3 was added in 1964, and Bore 4 – excavated with the New Austrian Tunnelling Method
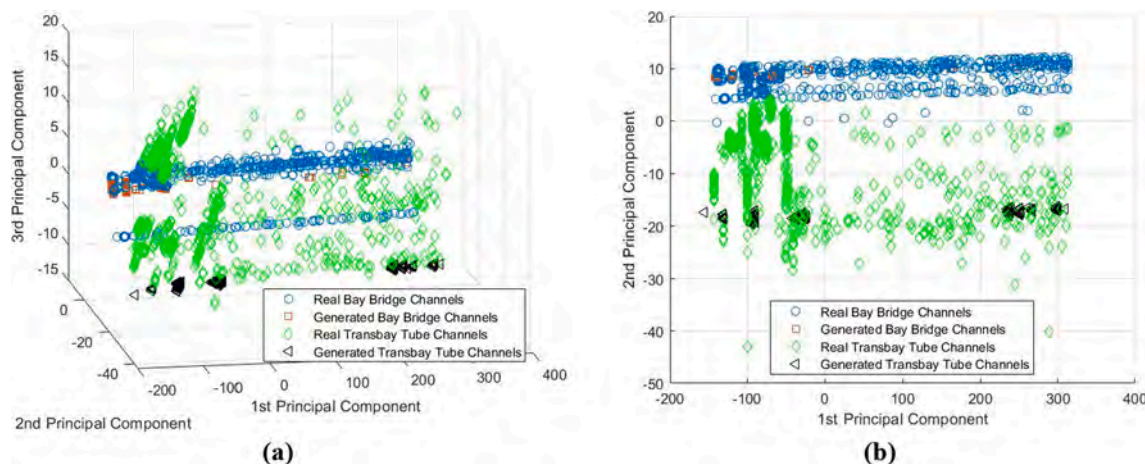
Fig. 4. BB vs TT. PCA scatterplots: **(a)** the 3D representation in the three main components and **(b)** the 2D representation in the first versus second main component plane.
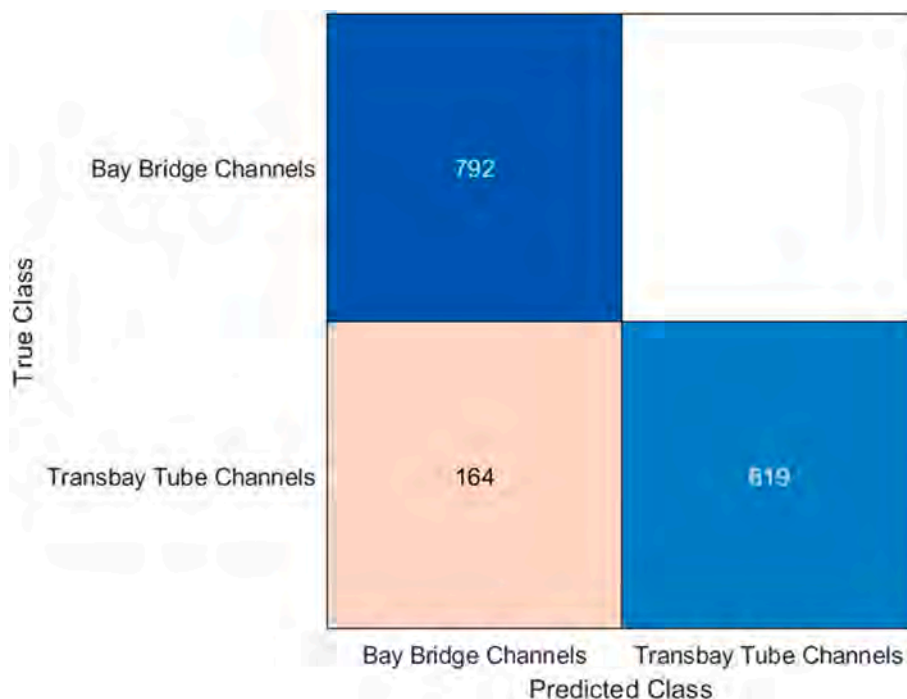

Fig. 5. BB vs TT. Confusion matrix representing the SVM's performance.

(NATM) – finally entered service in 2013. Among them, the most recent tunnels (i.e. Bore 3 and 4) are equipped with monitoring systems. Particularly, Bore 4, which accommodates two traffic lanes, has 21 sensors located at five different cross-sections, constituting the station called CE58540, while Bore 3 only has three instrumented sections. In this study, for simplicity, only the fourth bore is considered and will be referred to simply as the Caldecott Tunnel.

Structurally, Bore 4 is 1036 m long with a cross-section 15.2 m wide. It was built using cast-in-place reinforced concrete placed upon a waterproof PVC geomembrane supported by a geotextile (Nitschke et al., n.d.; Thapa et al., n.d.).

Fig. 3 shows images of the three previously described infrastructures.

3.4. Earthquakes considered

The CESMD uploads, on its website, records of the ground and structural responses caused by earthquake-strong motion for engineering purposes. The seismic data have been retrieved from their database. The type of data uploaded can be of two types: the first is known as the Internet Quick Report (IQR), which includes data related to earthquakes posted online within a few minutes of the seismic event. The second is a more comprehensive report called Internet Data Report (IDR), which contains a reviewed version of the seismic data within supporting thematic maps.

The first and main event analysed in this study is the Berkeley Earthquake of 04 January 2018[2] (hereinafter, BE18), which had a magnitude of 4.4 MW and a depth of 12.3 km. The epicentre was only 8.51 km and 10.78 km away from the BB and the TT (considering the position as per the longitude and latitude assigned to the respective stations in the CESMD dataset). Of course, such very near-fault ground
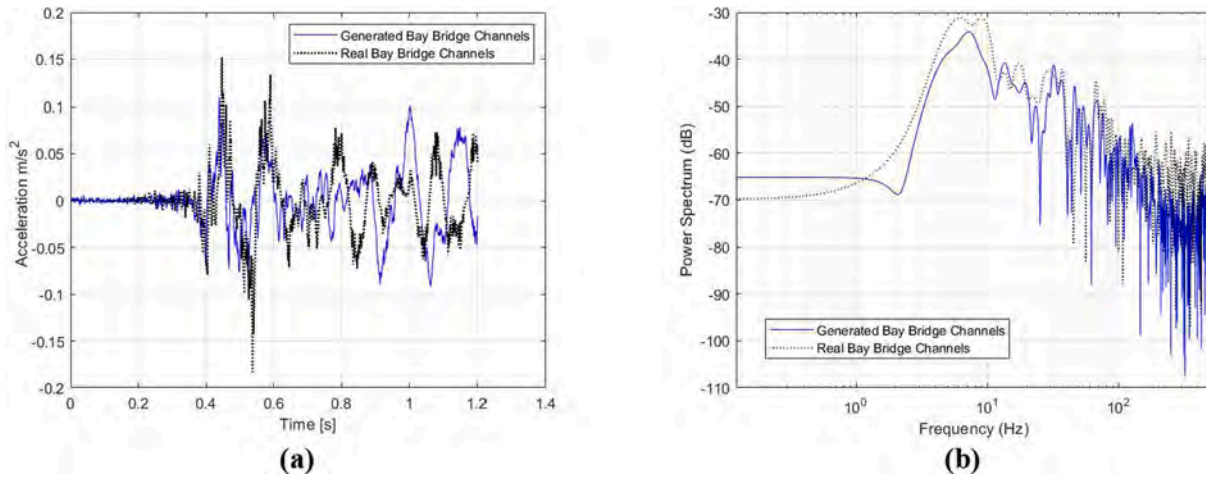
---

[2] https://earthquake.usgs.gov/earthquakes/eventpage/nc72948801/executive.

Fig. 6. BB vs TT. Comparison between the real and generated data in the time domain **(a)** and in terms of the power spectra **(b)**. Comparison between one example of BB channels.
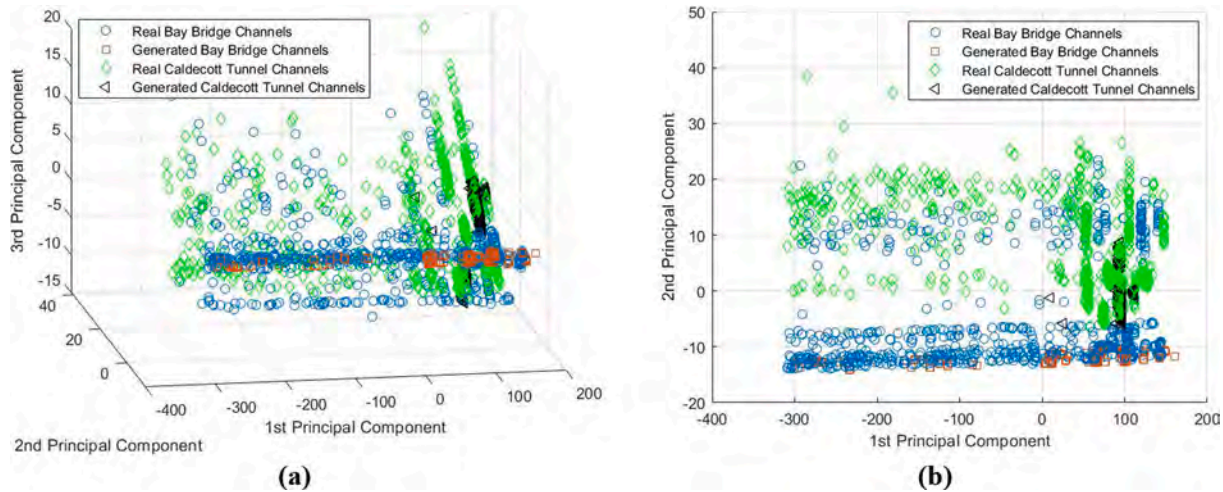

Fig. 7. BB vs TT (pile included). PCA scatterplots: (a) the 3D representation in the three main components and (b) the 2D representation in the first versus second main component plane.

motions tend to increase the expected damage to civil structures if compared to events with the same intensity but originated further afield.

The other earthquakes that have been considered are the Piedmont Earthquake of 17 August 2015[3] (PE15), with a magnitude of 4.0 M_{w} and a depth of 4.7 km and the South Napa Earthquake of 24 August 2014[4] (SN14), with a magnitude of 6.0 M_{w} and a depth of 11.1 km. The recorded data of PE15 and SN14 are available only for the two case studies BB (station CE58601) and CT (station CE58540), but not for TT, where BE18 is the only available strong motion. Further information on the sources and validity of the data used could not be provided since it is not available in the data source.

4. Analysed pairs

Each infrastructure is equipped with a monitoring system composed of accelerometers distributed on the structure itself. In the CESMD inventory, each sensor has its name expressed by a progressive

numeration. In this work, each transversal sensor has been renumbered for better understanding. The old and new numbering are shown in Table 1. The corresponding sensor layouts are available in the drawings of Appendix A.

The aim of this study is (also) to compare directly over- and underground infrastructures, as well as different typologies of underground infrastructures (deep road tunnels vs shallow underwater rail tunnels). For this reason, also considering the limited number of available seismic events, the three case studies have been compared in pairs. In each pair, the recorded time series of acceleration of two infrastructures under the effect of the same earthquakes are considered.

That resulted in six different combinations, with their peculiarities in terms of infrastructures compared, channels selected, and earthquakes considered. These changes allow us to determine the variation in the algorithm's performance. The pairs are listed as follows:

I. **Bay Bridge vs Transbay Tube:** for BB, all the transversal channels selected on the deck are considered; for TT, all the selected transversal channels are used as well;

II. **Bay Bridge vs Transbay Tube (pile included):** for BB, all the transversal channels selected on the deck plus the ones located on Pier E6E are considered; for TT, all the selected transversal channels are used;
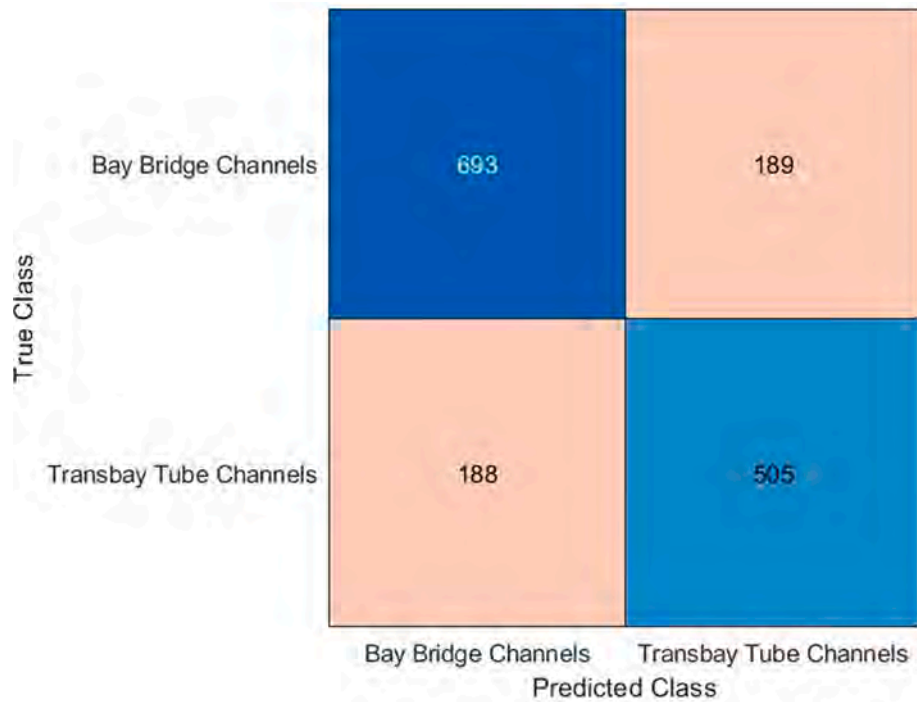
---

[3] https://earthquake.usgs.gov/earthquakes/eventpage/NC72507396/executive.

[4] https://earthquake.usgs.gov/earthquakes/eventpage/NC72282711/executive.

Fig. 8. BB vs TT (pile included). Confusion matrix representing the SVM's performance.
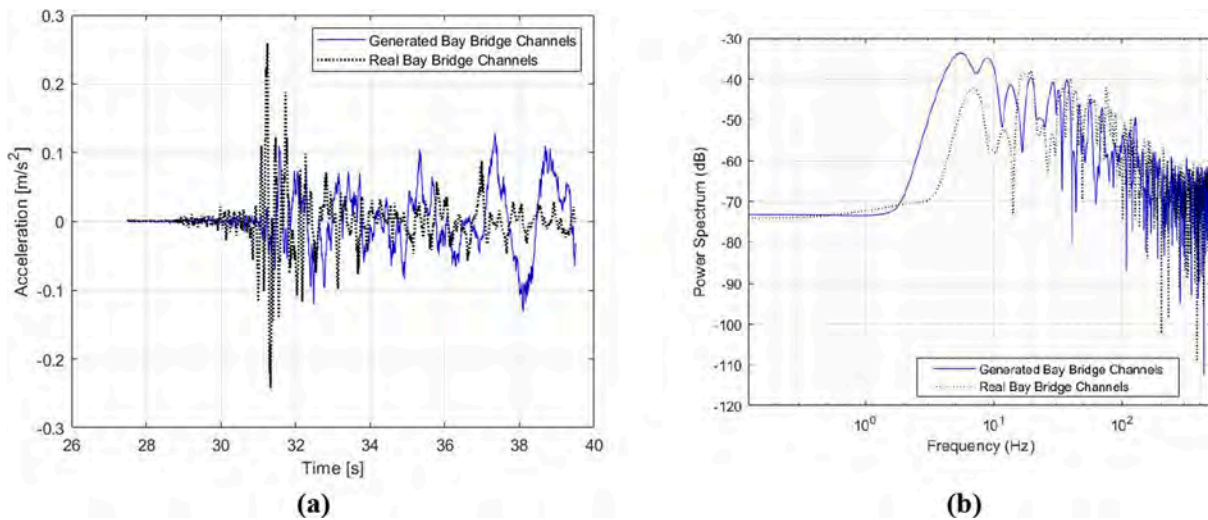

Fig. 9. BB vs TT (pile included). Comparison between the real and generated data in the time domain **(a)** and in terms of the power spectra **(b)**. Comparison between one example of BB channels.

III. **Bay Bridge vs Caldecott Tunnel:** for BB, all the transversal channels selected on the deck are considered; for CT, all the selected transversal channels are used as well;

IV. **Bay Bridge vs Caldecott Tunnel (pile included):** for BB, all the transversal channels selected on the deck plus the ones located on Pier E6E are considered; for CT, all the selected transversal channels are used;

V. **Transbay Tube vs Caldecott Tunnel**: all the selected transversal channels are used for both TT and CT;

VI. **Bay Bridge vs Transbay Tube (all seismic responses):** lastly, another case has been studied; the difference from I is the use of data coming from different earthquakes for the BB.

A summary of the characteristics of these pairs is shown in Table 2.

The rationale for these choices is as follows. The first analysis (I) compares the readings from the bridge deck (i.e. from the superstructure only) to the ones of the nearby underwater tunnel. The second analysis (II) adds the readings from the sensors BB-1, BB-2, and BB-3, which are located in the substructure on one of the piles, Pier E6E, respectively, at −28.5 m, −59.9 m, and −78.4 m. Analyses III and IV mirror I and II, respectively, replacing the TT with Bore 4 of the CT. Analysis V directly compare the two underground infrastructures. In contrast, the last analysis (VI) is identical to the first (I) but adds the time series collected during two other earthquakes recorded at the BB station.

The signals of the BB and TT are recorded with the same sampling time of $\Delta t = 0.010$ s. That enables a perfect comparison without any
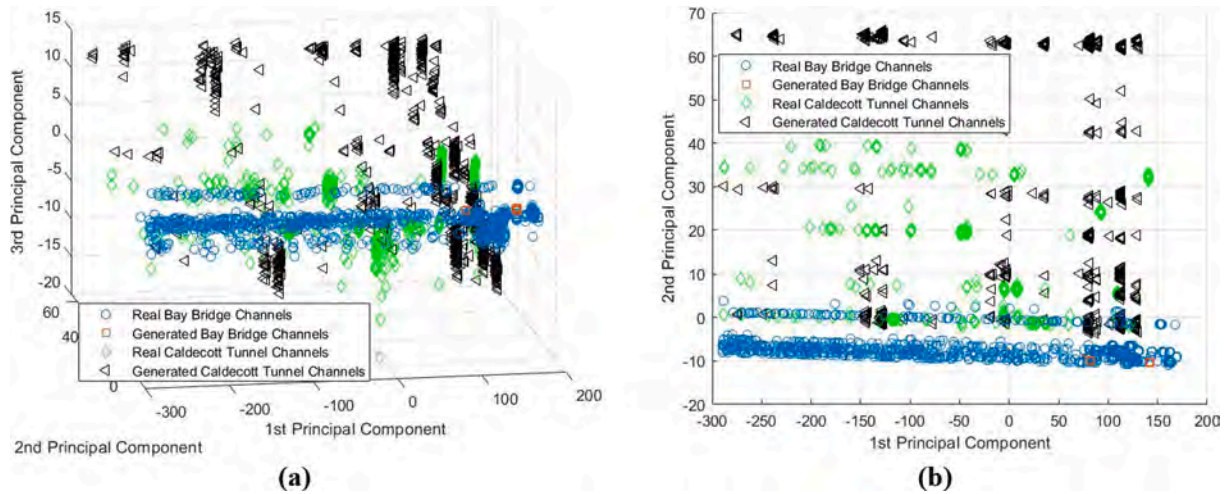
Fig. 10. BB vs CT. PCA scatterplots: (a) the 3D representation in the three main components and (b) the 2D representation in the first versus second main component plane.
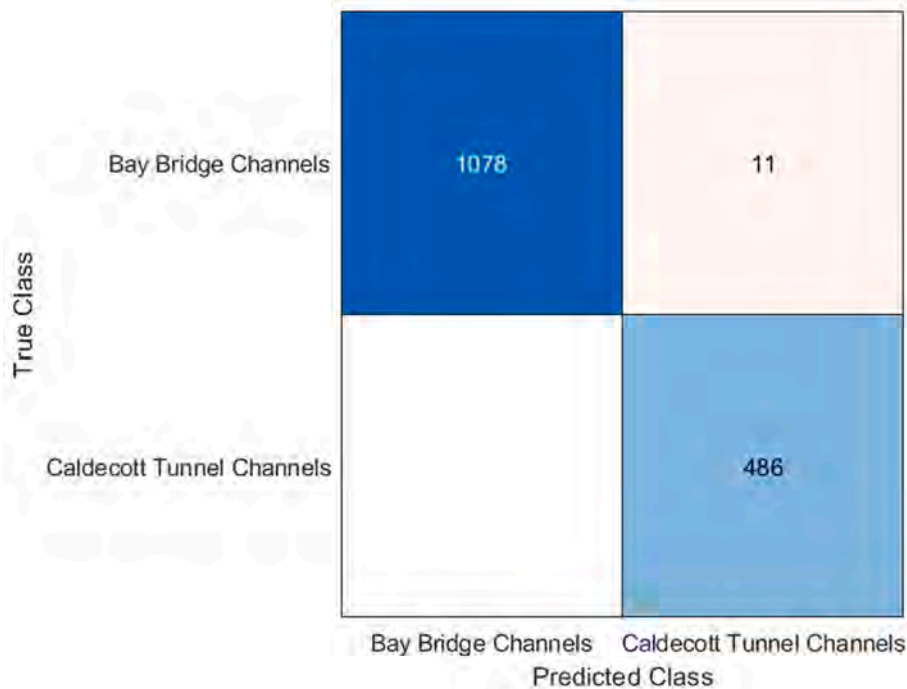

Fig. 11. BB vs CT. Confusion matrix representing the SVM's performance.

need for pre-processing. However, in the case of the CT, the original time step was $\Delta t = 0.005$ s. Thus, these latter time series were decimated to meet the same sampling frequency.

5. Results

The algorithm was run on a Hewlett Packard (HP®) Z4 workstation with the following features: INTEL® XEON® W processor, 22 TB storage capacity, and 256 GB memory. On average, for each pair, it took 7 to 8 hours to train the network and obtain the results of the post-processing phase. In the following subchapter, the results of the data generation and binary classification procedure are presented and discussed for the six different pairs considered in this study. In all cases, the training

consisted of 1000 epochs and 6000 iterations, after which the process was stopped.

Pair I: Bay Bridge vs Transbay Tube.

The analysis of the generated data starts from the PCA results. These are graphically depicted in Fig. 4, plotted in the 3D space of the three principal components – PC1, PC2, and PC3. The percentage of energy contained in the first three PCs, with respect to the total energy, is 98.3 %. This very high percentage proves that PCA has effectively captured the dominant patterns and variations within the data, efficiently reducing the dimensionality of the data while retaining the most significant information. Hence, PC1, PC2, and PC3 offer a valid synthetic representation of the corresponding signals.

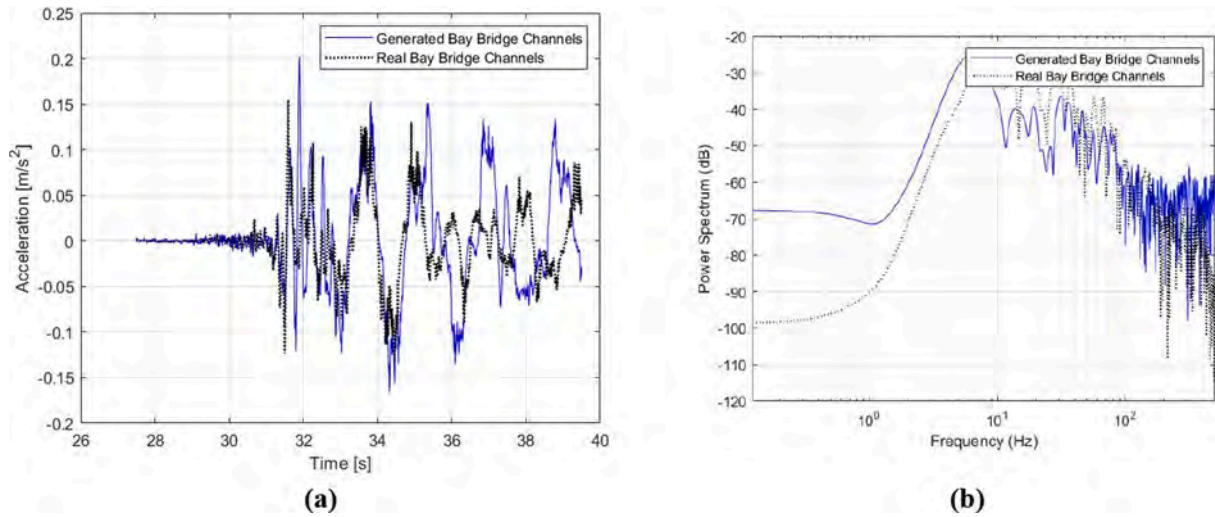It is possible to point out that the BB's records are almost parallel to

Fig. 12. BB vs CT. Comparison between the real and generated data in the time domain **(a)** and terms of the power spectra **(b)**. Comparison between one example of BB channels.
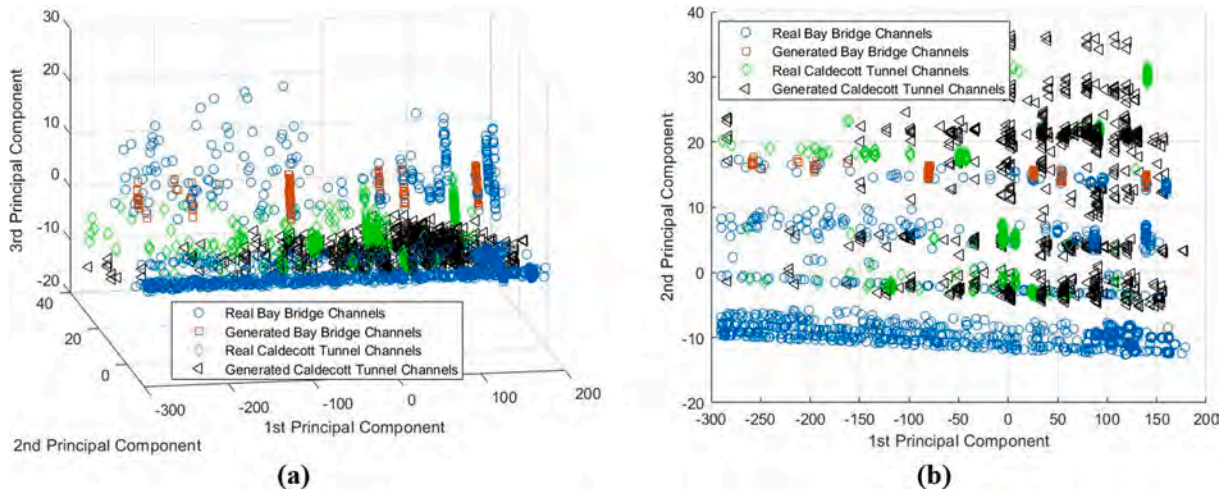

Fig. 13. BB vs CT (pile included). PCA scatterplots: (a) the 3D representation in the three main components and (b) the 2D representation in the first versus second main component plane.

the PC1 and that the TT's records are parallel to the PC2, even if there is more spread in the space of the three selected PCs. Nevertheless, these two alignments and their orthogonality highlight that the two case studies behave distinctly for the same seismic input.

Fig. 5 shows the confusion matrix resulting from the SVM analysis. Based on the features retrieved from the generated data, the SVM performs a binary classification to assign labels to the real ones.

The performance metrics adopted in this classification are accuracy, precision, recall, and F_1 score, following their conventional meaning in ML classification tasks.

In this case, it has reached an accuracy of 89.6 %, a precision of 100 %, a recall of 82.8 % and an F_1 score of 90.6 %. In particular, all the BB channels are effectively and correctly predicted; on the other hand, 20 % of the TT channels have been mispredicted.

As the last step of the analysis, the direct comparison between the real and generated data is performed in the time and frequency domains. Fig. 6 (a) plots one example of a generated acceleration time series from the BB case against time. A real acceleration time series is also superimposed in the same graph for visual comparison. Please note that since

all input (real) time series were standardised, the output (generated) time histories also have zero mean and unit standard deviation. For this reason, the algorithm reverts the standardisation process performed on the original signals, multiplying by the standard deviation and adding the mean. Thus, the generated time series are not dimensionless but can be expressed in terms of (m/s^2), as reported in Fig. 6 (a) and the similar Figures in the following subsections.

As can be seen, it is impossible to distinguish by the naked eye between the real and the generated data; both signals have similar amplitude and oscillation patterns. As shown in the following analyses, G automatically learns some peculiarities of a typical seismic response, such as the small-amplitude vibrations in the pre-shock initial stage and the large-amplitude vibrations afterwards. In the time domain, the resemblance can also be quantitatively estimated in terms of key waveform metrics, for instance, considering the maximum value of peak-to-peak amplitude (pk-pk), i.e. the difference between the highest and the lowest values in a signal, and the maximum peak-to-zero amplitude (pk-0), i.e. the highest value of the amplitude of the same signal. In particular, in Fig. 6, the maximum pk-pk is 0.201 and 0.329 for
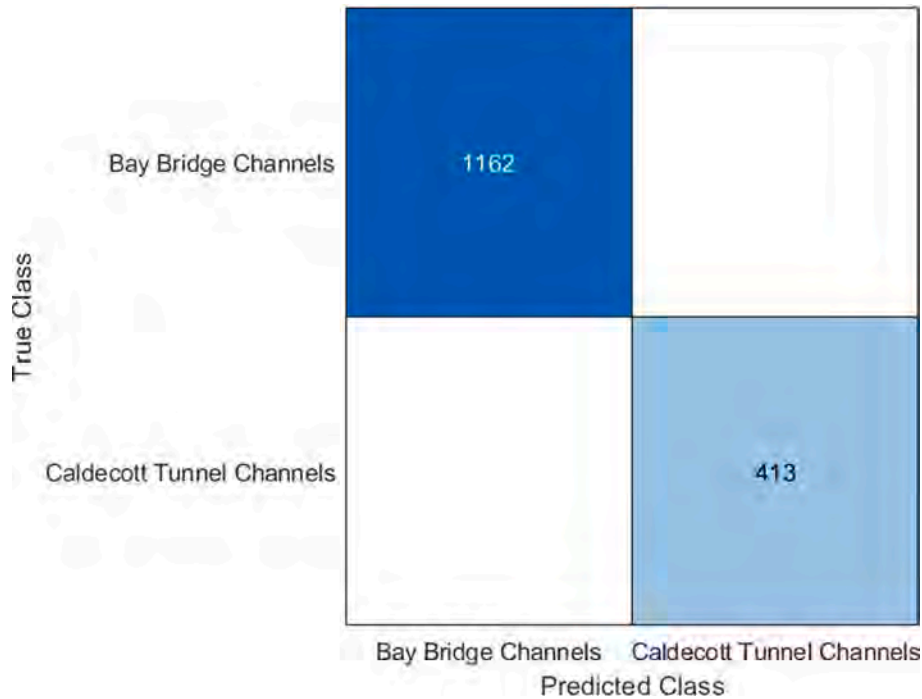
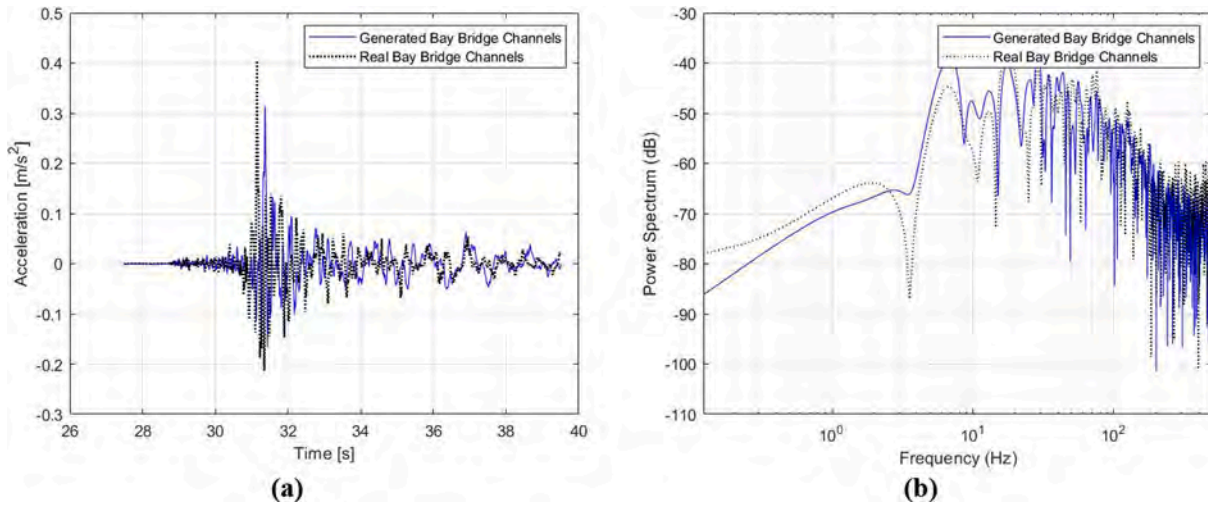**Fig. 14.** BB vs CT (pile included). Confusion matrix representing the SVM's performance.

Fig. 15. BB vs CT (pile included). Comparison between the real and generated data in the time domain **(a)** and in terms of the power spectra **(b)**. Comparison between one example of BB channels.

the generated and the real data, respectively, and the maximum pk-0 amplitude is 0.110 and 0.169. The overall good similarity of these values confirms the results' consistency.

More importantly, the generated data show good comparability in the frequency domain – see Fig. 6 (b). This spectral compatibility allows for the use of the proposed data generation methodology in damage detection approaches (Martucci et al., 2023), especially frequency-based ones.

Pair II: Bay Bridge vs Transbay Tube (pile included).

In Fig. 7, the representation obtained in the space of the three PCs is reported. Similar to the previous case, the energy contained in the three components corresponds to 98.3 % of the total energy. Also, as in the first analysis, it is possible to point out that the BB's signals (both

measured and generated) are almost parallel to the PC1, while the TT's signals are parallel to the PC2.

The results of the SVM analysis are reported in the confusion matrix of Fig. 8. Both cases present a non-negligible level of misidentifications. Specifically, the SVM reached an accuracy of 76.1 %; in comparison to the previous analysis, the precision fell from 100 % to 78.6 % and the recall from 82.8 % to 78.7 %. F_1 score dropped about 10 %, settling at 78.6 %. That is to say, introducing the channels located on the pile of Pier E6E led to a reduction in the effectiveness of pattern recognition. This is reflected in the decrease in performance metrics compared to the previous analysis. In summary, the introduction of underground channels has diminished the overall differences in terms of features between the two datasets.
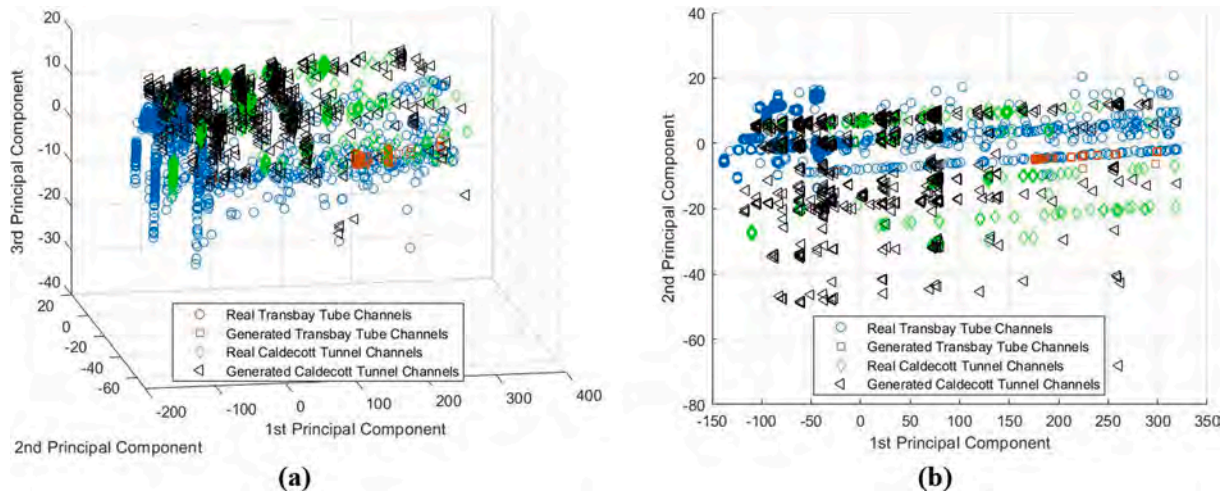
Fig. 16. TT vs CT. PCA scatterplots: (a) the 3D representation in the three main components and (b) the 2D representation in the first versus second main component plane.
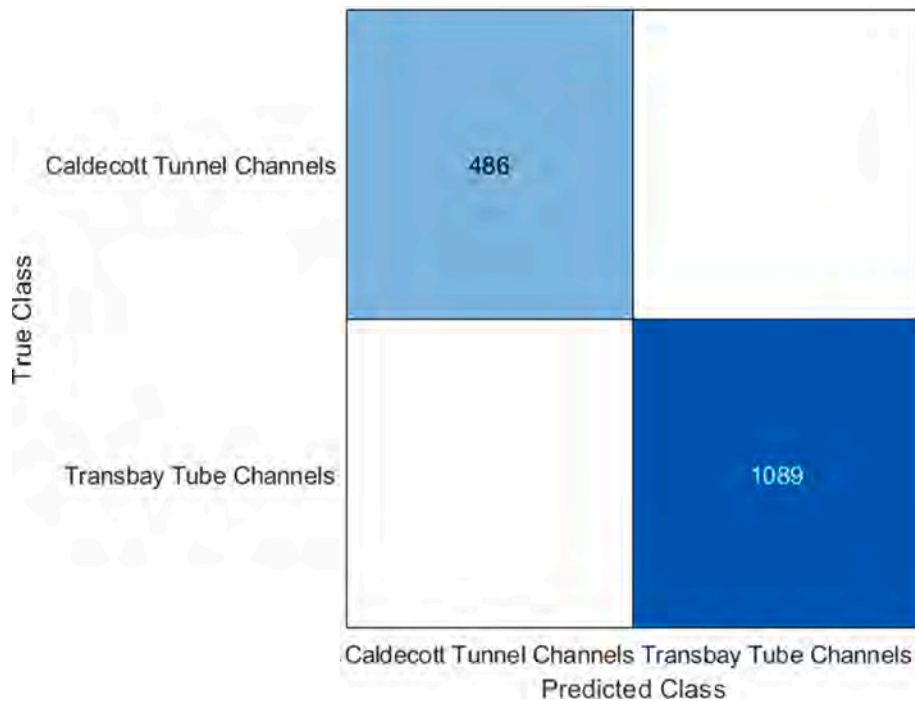

Fig. 17. TT vs CT. Confusion matrix representing the SVM's performance.

The final step of the analysis involves a direct comparison between real and generated data in the time domain and frequency domain, represented in Fig. 9. The maximum pk-pk amplitude is 0.260 and 0.500 for the generated and the real data, respectively, while the maximum pk-0 amplitude is 0.131 and 0.0.258.

Pair III: Bay Bridge vs Caldecott Tunnel.

Fig. 10 illustrates the scatterplot representations obtained performing the PCA. The energy contained in the first three components relative to the total energy amounts to circa 98 %. It is possible to point out that the BB's signals are slightly inclined in the 3D space but well aligned with the PC1, while the CT's signals run parallel to the PC2.

The confusion matrix coming is shown in Fig. 11. Notably, there is almost perfect precision in predicting the two distinct classes. Particularly, the BB has only 11 cases mislabelled. The SVM reached a very high prediction accuracy of 99.3 %, as well as a precision of 98.9 %, a recall of 100 % and an F_1 score of 99.5 %. Most probably, the increase in the

distinction is due to a combination of different structural typologies, different geological conditions in which the two infrastructures are located, and geographic distance. In this pair, all the performance metrics reach an outstanding high value, almost a flawless score.

The final step of the analysis involves a direct comparison between real and generated data in the time domain and frequency domain, as depicted in Fig. 12. In this case, the maximum pk-pk amplitude is 0.366 and 0.290 for the generated and the real data, respectively, and the maximum pk-0 amplitude stands at 0.201 and 0.155.

Pair IV: Bay Bridge vs Caldecott Tunnel (pile included).

The results of the PCA are illustrated in Fig. 13. As for all the analyses performed, the ratio of the energy contained in the three components with respect to the total energy is very high at 98,3 %. These scatterplots show that the BB's records are parallel to the PC1 and that the CT's records are oriented as the PC2.

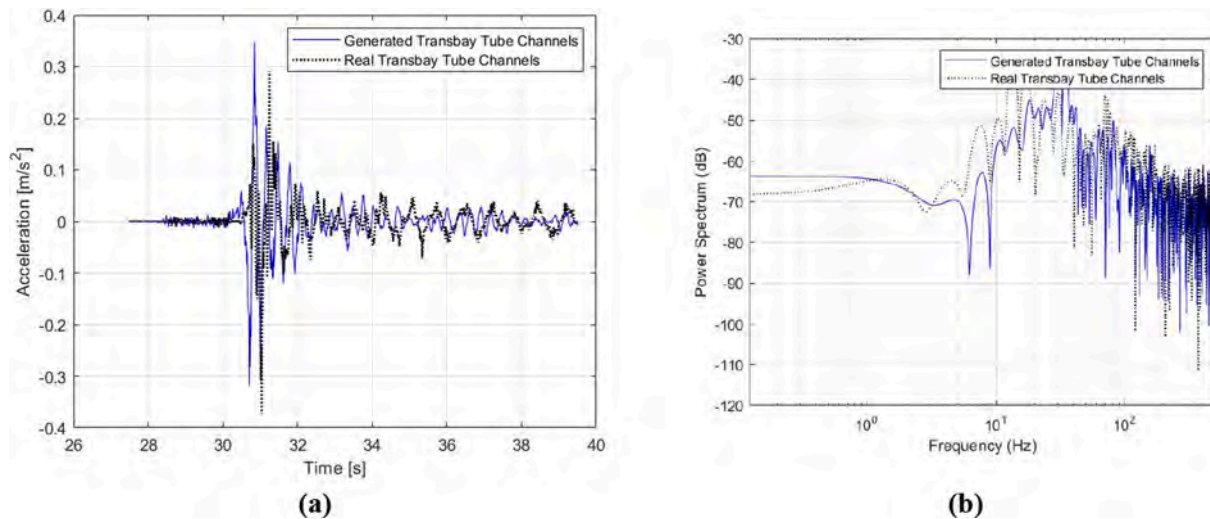In Fig. 14, the results of the SVM analysis are presented. Strikingly,

Fig. 18. TT vs CT. Comparison between the real and generated data in the time domain **(a)** and in terms of the power spectra **(b)**. Comparison between one example of TT's channels.
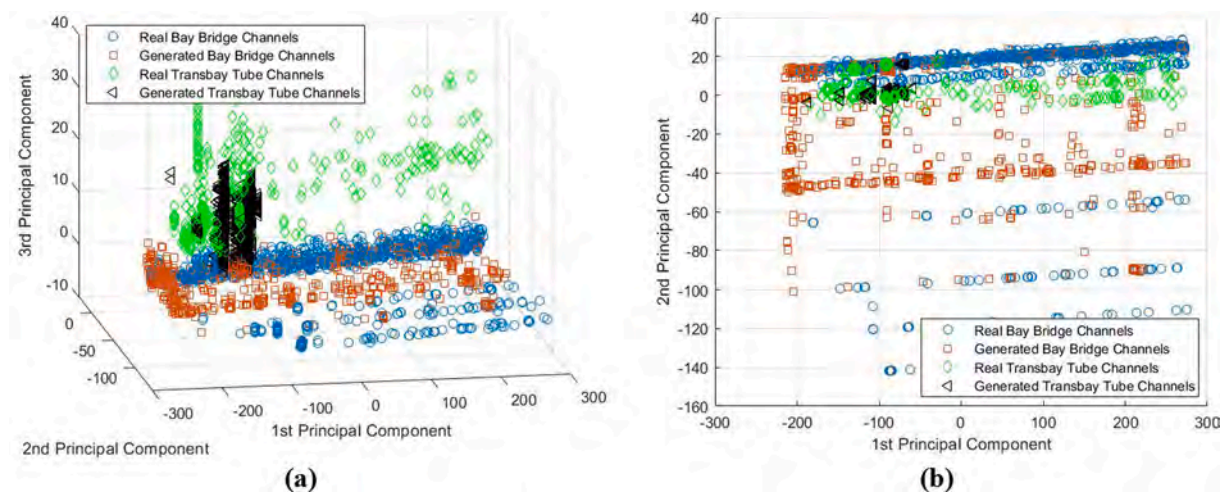

Fig. 19. BB vs TT (all seismic responses). PCA scatterplots: (a) the 3D representation in the three main components and (b) the 2D representation in the first versus second main component plane**.**

the SVM exhibits a perfect prediction capability in this case. In particular, all the BB and the CT signals are correctly labelled, with no mis-identifications. That suggests that the characteristics of the BB's and CT's acceleration signals were flawlessly captured during the algorithm's training.

Compared to the previous case, the accuracy increases from 99 % to perfect (100 %) prediction. The precision and recall increase as well, respectively, from 99.3 % and 98.9 % to 100 %, as all performance metrics reach a flawless score. The F_1 score flawlessly reaches 100 %. These results contrast with the first two analyses, where the inclusion of Pier E6E data in the BB dataset worsened the SVM binary classification between BB and TT. In this case, including the same data improved the SVM results between BB and CT. One possible explanation is that the instrumented bridge pile is very close to the TT and immersed in very similar soils, which is, instead, very different from the geological conditions of the CT. Hence, the same data that acted as a source of similarity in the first comparison are here a further source of distinction.

One example of real and generated data are juxtaposed in the time and frequency domain in Fig. 15. The maximum pk-pk amplitude is 0.481 and 0.344 for the generated and the real data, respectively; in the

same order, the pk-0 amplitude reaches 0.314 and 0.197.

Pair V: Transbay Tube vs *Caldecott Tunnel.*

In Fig. 16, the PCA results are plotted. The percentage of energy contained in the first three PCs is 98.1 % of the total. By examining these scatterplots, it is noticeable that both the real data of the TT and the CT exhibit a slight inclination with respect to the PC1 but run parallel to each other.

Fig. 17 depicts the confusion matrix obtained from SVM analysis. In this instance, a flawless prediction of the two classes is attained. In both cases, the predictions made by the SVM are correct without any mis-labels. As for the previous analysis, the SVM reached an accuracy, a precision, a recall and an F_1 score of 100 %, i.e., a perfect score. Hence, in the case of the comparison between the two tunnels, most probably due to the very different geological conditions, optimum separability is reached, thus highlighting very distinct seismic behaviours to the same strong motion.

An example of a direct comparison between real and generated data in the time domain and frequency domain is shown in Fig. 18. Considering the waveform features of interest, these are very similar as well: the maximum pk-pk amplitude is 0.665 and 0.664 for the generated and
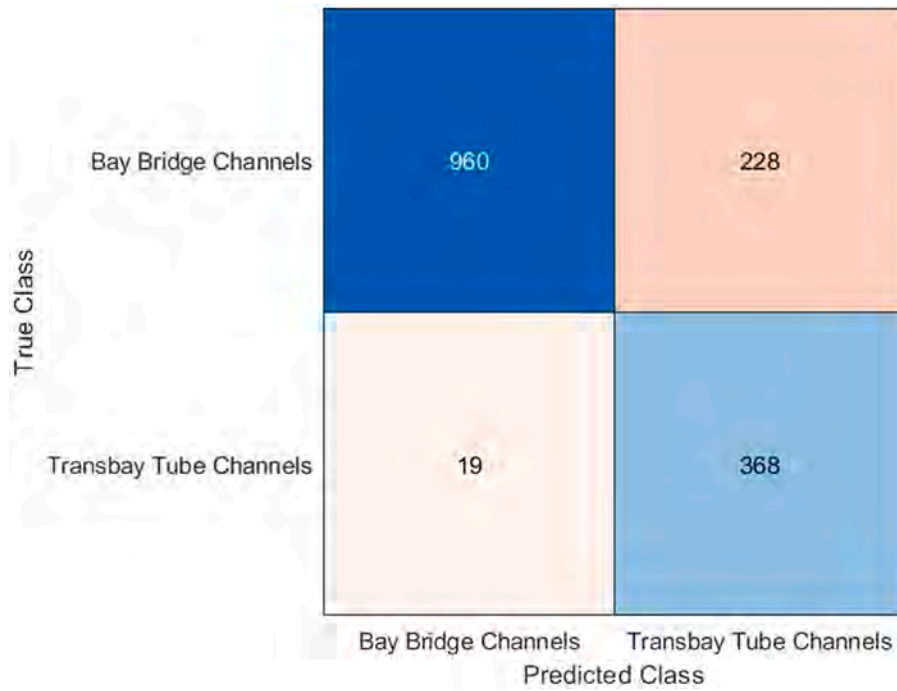
Fig. 20. BB vs TT (all seismic responses). Confusion matrix representing the SVM's performance.
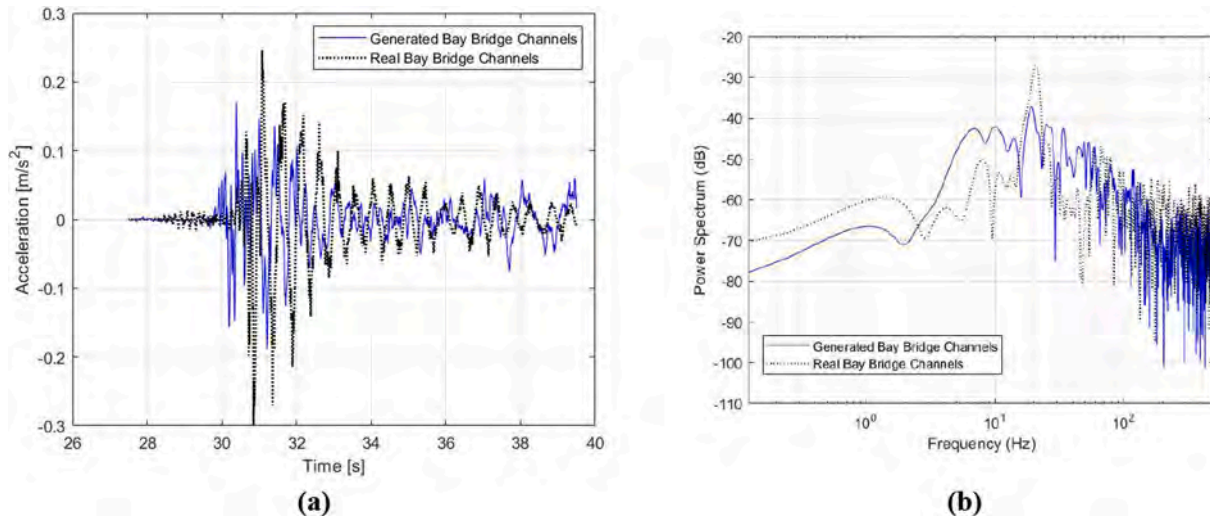

Fig. 21. BB vs TT (all seismic responses). Comparison between the real and generated data in the time domain **(a)** and in terms of the power spectra **(b)**. Comparison between one example of BB channels.

the real data, respectively, while the maximum pk-0 amplitude is 0.347 and 0.373.

Pair VI: Bay Bridge vs Transbay Tube (all seismic responses).

In Fig. 19, the PCA of interest is represented. The energy contained in the three components with respect to the total energy is 98.4 %. As for the first and second analyses, the BB's records are almost parallel to the PC1. However, unlike the previous cases, in this instance, the TT's records align with the PC3 rather than the second one. It is clear, then, that

introducing a more heterogeneous dataset with respect to the two previous cases leads to a notable variation in the results of the PCA and of the PCs.

Fig. 20 shows the confusion matrix retrieved with the SVM analysis. Notably, introducing a more heterogeneous dataset for the label corresponding to the BB has led to a reduction of almost 5 % in prediction accuracy compared to the first analysis, down to 84.3 %. Considering the other performance metrics, the obtained precision is 80.8 %, and the

recall is 98.0 %. The F_1 score is 88.6 %, slightly decreasing compared with pair I. Comparing these results with the ones from pair I, it is possible to denote a reduction in the precision (about 20 %) but, conversely, an increase of 18 % in recall.

As for all the previous analyses, the final step is a direct comparison between real and generated data in the time and frequency domain, as represented in Fig. 21. The maximum pk-pk amplitude is 0.359 and 0.545 for the generated and the real data, respectively, while the maximum pk-0 amplitude stands at 0.189 and 0.299.

6. Conclusions

Recent events, such as the Hualien County earthquake on April 3rd, 2024, reminded the scientific community of the risks posed by earthquakes to tunnels and other underground spaces, which are often overlooked.

This research work aimed to address the obstacle posed by the lack of experimental seismic data, accounting for the different dynamic responses of viaducts, underwater tunnels in soft soil, and mountain tunnels in rock. Secondly, related to this last aspect, it aimed to compare the seismic behaviour of these over- and underground infrastructures, especially below-ground infrastructures of different kinds.

A data generation process has been implemented to overcome the data scarcity issue, resorting to the ML technique known as CGAN. The goodness of the so-generated data has been confirmed and visualised in the time and frequency domains, as well as through PCA in the three main PCs.

Then, using the generated data as the training dataset, an SVM binary classifier has been proven capable of discerning the real data (i.e. the recorded dynamic responses) of the three case studies – the Bay Bridge, a deep road tunnel known as the Bore 4 of the Caldecott Tunnel, and a shallow underwater tunnel known as the Transbay Tube. These three target systems are all geographically nearby, located in the San Francisco Bay Area, but are characterised by different geological and structural conditions. That highlights the differences between the vibrational responses of these infrastructures to the same strong motions.

Specifically, six different pairwise analyses have been conducted, considering several sensor configurations and seismic events. The main outcomes can be summarised as follows:

- In all the cases, the energy contained in the first three components obtained performing the PCA amounts to approximately 98 %. Plotting the three components mentioned above makes it possible to obtain the scatterplots of the PCA, in which it is possible to identify the alignment of the data of a structure with respect to a certain principal component and how they are spread in the space. In all analyses, this confirmed the effectiveness of the data generation procedure.
- The accuracy of the confusion matrix, obtained with SVM binary classification, varies between 76.1 % and 100 %, with an average of 91.55 %. Particularly, it is possible to denote that the precision is higher when studying infrastructures located in different geological conditions – for instance, the results of pairs III (BB vs CT), IV (BB vs CT), and V (CT vs TT) – than when different types of nearby infrastructures are compared – e.g., pair I (BB vs TT), II (BB vs TT), and VI (BB vs TT). That indicates a dominant effect of the geotechnical

conditions on the key signal features learnt by the deep neural network.
- The precision, recall, and F_1 score reach important results as well, varying (in the same order) between 78.6 % and 100 % (average precision: 93.05 %), 78.7 % and 100 % (average recall: 93.25 %), and 78.6 % and 100 % (average F1 score: 92.88 %).
- Visual comparison in both time and frequency domains confirms the similarity of real and generated data as well. Considering the results of pk-pk and pk-0 amplitude, there is a slight inconsistency in the results between the real and the generated data, but time domain comparability is reported for completeness' sake only. For practical purposes, frequency domain-compliant generated signals were the main goal to achieve.

Considering the obtained results, it is possible to affirm that both the data generation and data classification procedures performed well in all the analyses carried out on the three case studies. The main limitation of this work is related to data scarcity, both in terms of available strong motion datasets and in terms of available infrastructures located in the same area. Hopefully, these limitations in future will become less impactful when monitoring becomes more common and more infrastructures above and below ground will be instrumented.

In future, the research aims to numerically assess the generated earthquake data, developing Finite Element Models (FEMs) of the target infrastructures and applying the recorded and synthetic earthquakes to them, investigating their effects.

Data availability statement

All the experimental data were recovered from Center for Engineering Strong Motion Data (CESMD) dataset and are publicly available on the website https://www.cesmd.org/index.html.

CRediT authorship contribution statement

M. Dalmasso: Writing – original draft, Visualization, Software, Methodology, Investigation, Formal analysis, Data curation. **M. Civera:** Writing – original draft, Visualization, Validation, Supervision, Software, Methodology, Data curation, Conceptualization. **V. De Biagi:** Writing – review & editing, Supervision, Conceptualization. **C. Surace:** Writing – review & editing, Supervision, Conceptualization. **B. Chiaia:** Writing – review & editing, Supervision, Resources, Project administration, Funding acquisition, Conceptualization.

Declaration of competing interest

The authors declare that they have no known competing financial interests or personal relationships that could have appeared to influence the work reported in this paper.

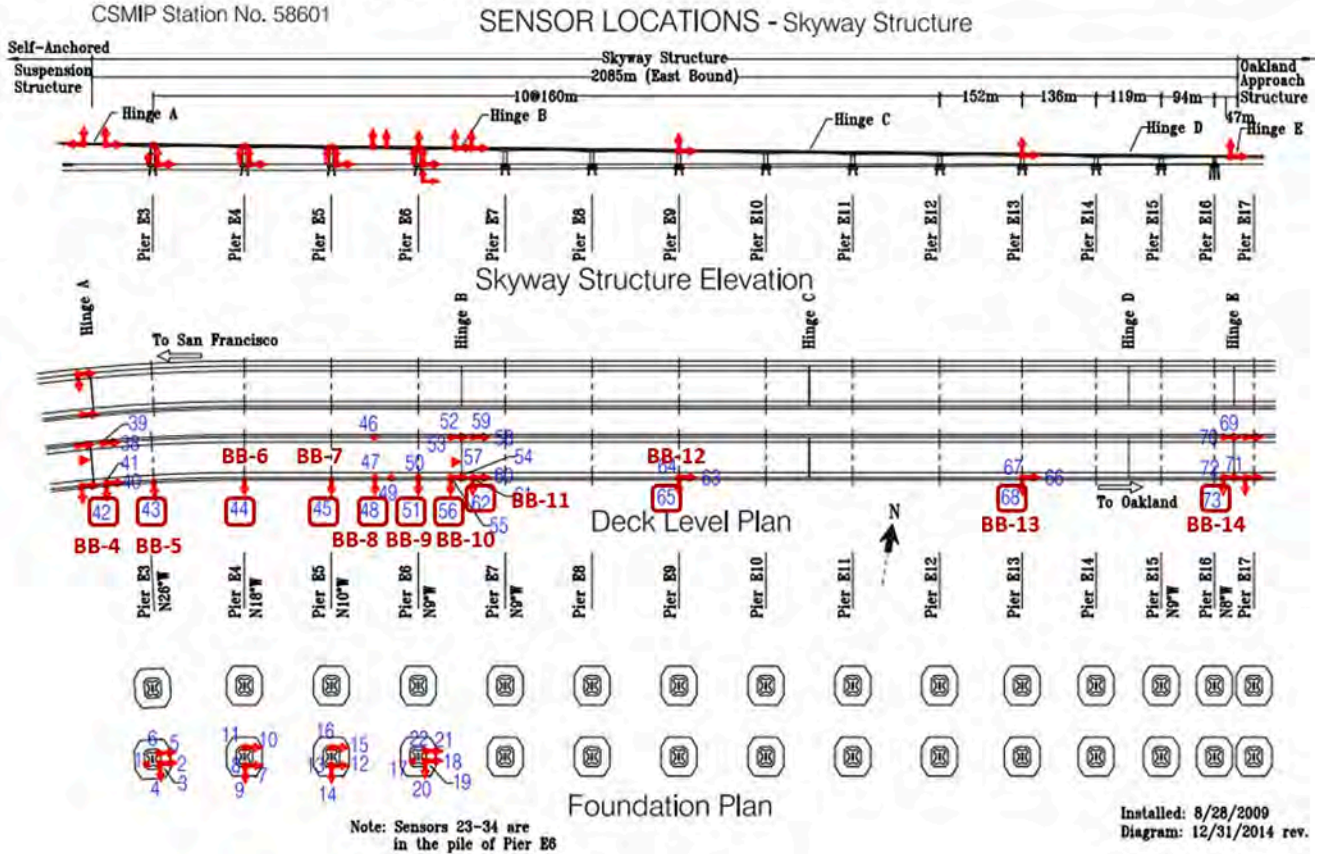## Acknowledgements

Appendix

Fig. A1. Locations of the channels of station 58601, corresponding to the sensor layout deployed on BB (Skyway portion of the Bay Bridge). Retrieved from: https://www.strongmotioncenter.org/NCESMD/photos/CGS/lllayouts/ll58601.pdf.
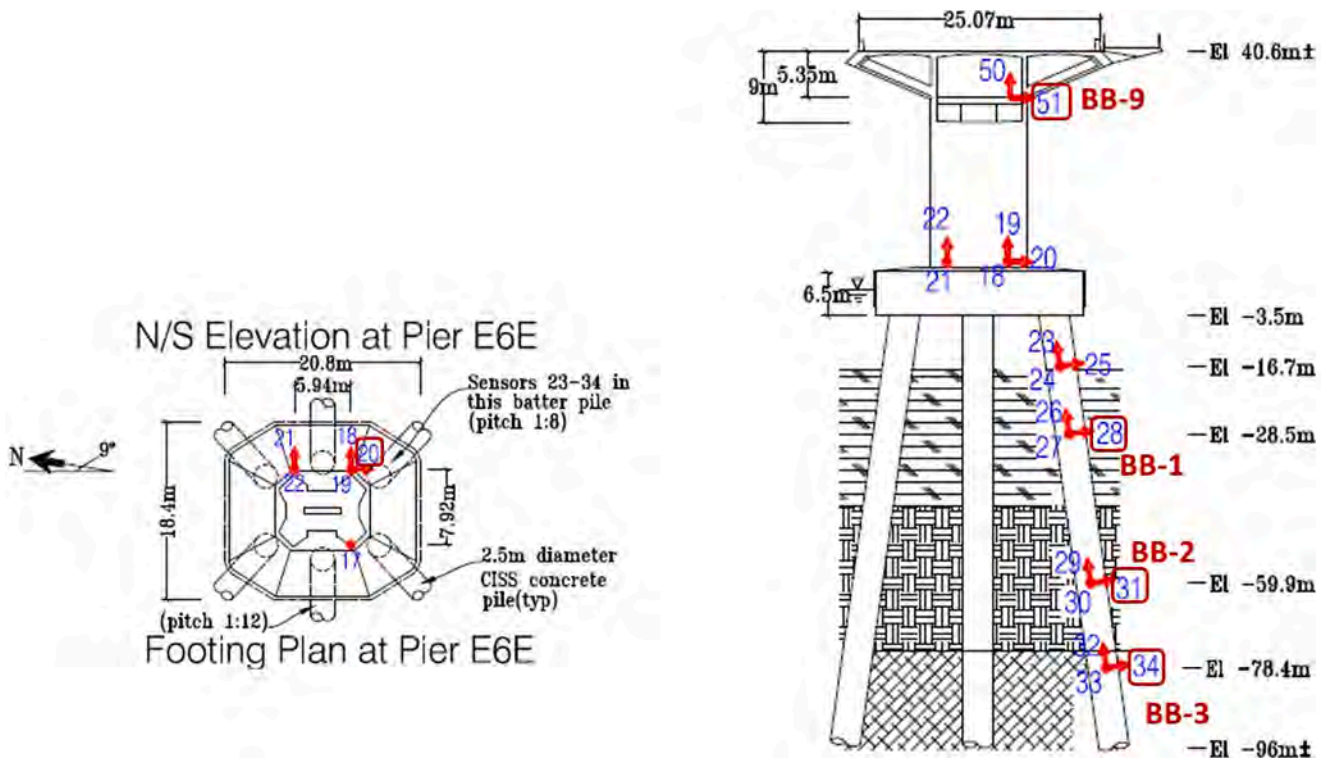
Fig. A2. BB's Pier E6E position of the channels: **(a)** side and **(b)** plan view. Retrieved from: https://www.strongmotioncenter.org/NCESMD/photos/CGS/lllayouts/ll58601.pdf.
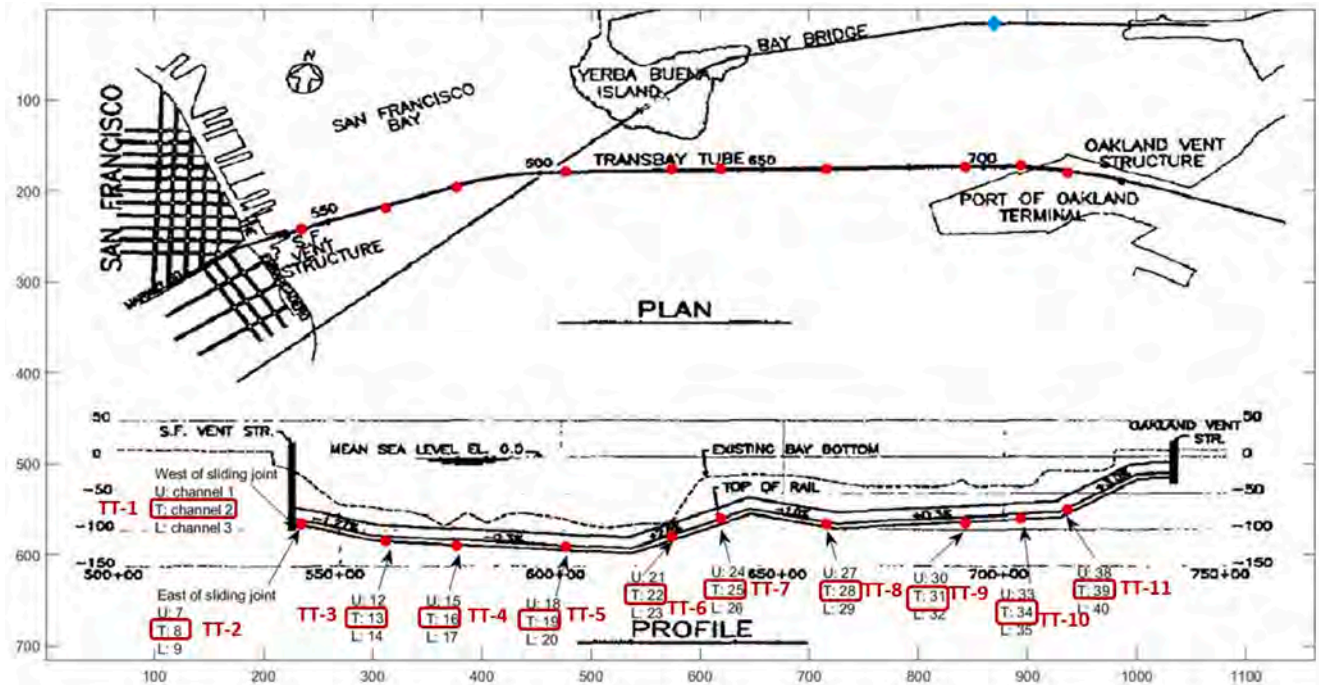

Fig. A3. Location of the sensor of TT (Transbay Tube) using a plan and a side view. Based on data retrieved by the Authors from several sources. For further details (Matteo Dalmasso et al., 2024).
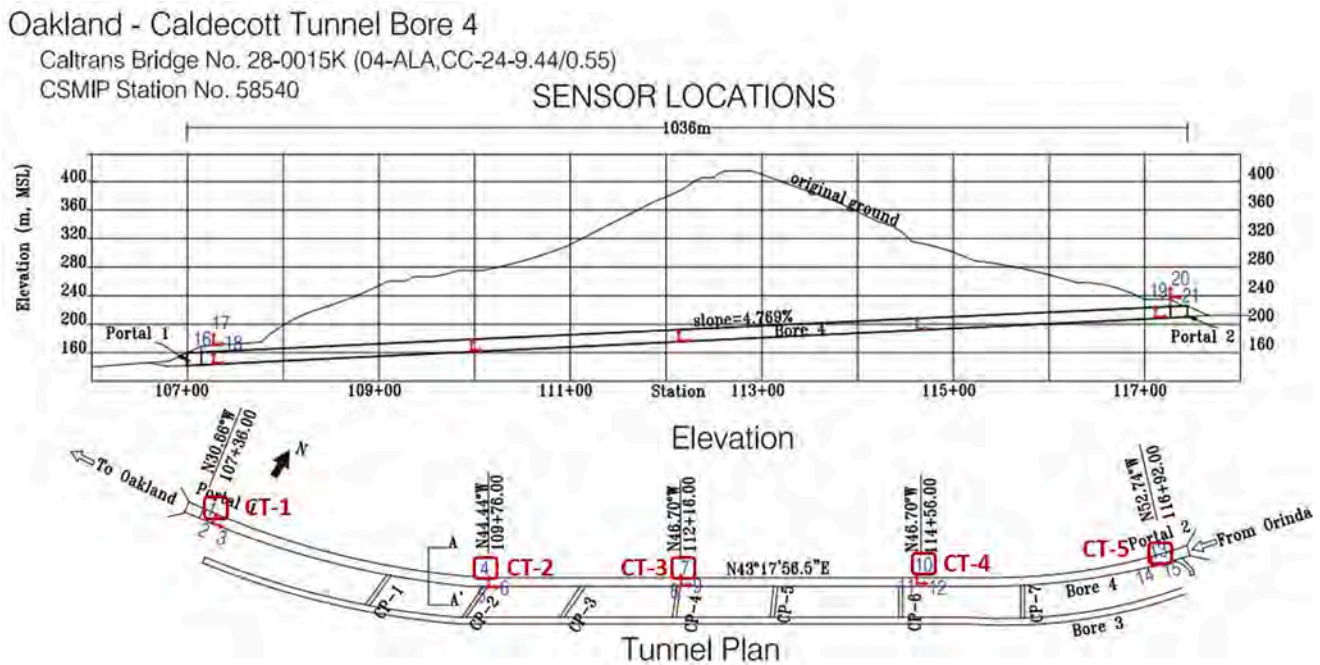
Fig. A4. Locations of the channels of station 58540, corresponding to the station located on CT (Bore 4 of the Caldecott Tunnel), using a plan and a side view. Retrieved from https://www.strongmotioncenter.org/NCESMD/photos/CGS/lllayouts/ll58540.pdf

Data availability

Data will be made available on request.

References

Asakura, T., Sato, Y., 1998. Mountain tunnels damage in the 1995 Hyogoken-nanbu Earthquake. *Quarterly Report-RTRI* 39.

Bana e Costa, C.A., Oliveira, C.S., Vieira, V., 2008. Prioritization of bridges and tunnels in earthquake risk mitigation using multicriteria decision analysis: Application to Lisbon. *Omega* 36 (3), 442–450. https://doi.org/10.1016/j.omega.2006.05.008.

Bilotta, E., Lanzano, G., Madabhushi, S.P.G., Silvestri, F., 2014. A numerical Round Robin on tunnels under seismic actions. *Acta Geotechnica* 9 (4), 563–579. https://doi.org/10.1007/s11440-014-0330-3.

Cervantes, J., Garcia-Lamont, F., Rodríguez-Mazahua, L., Lopez, A., 2020. A comprehensive survey on support vector machine classification: Applications, challenges and trends. *Neurocomputing* 408, 189–215. https://doi.org/10.1016/j.neucom.2019.10.118.

Chen, C.-H., Wang, T.-T., Jeng, F.-S., Huang, T.-H., 2012. Mechanisms causing seismic damage of tunnels at different depths. *Tunnelling and Underground Space Technology* 28, 31–40. https://doi.org/10.1016/j.tust.2011.09.001.

Cortes, C., Vapnik, V., 1995. Support-vector networks. *Machine Learning* 20 (3), 273–297. https://doi.org/10.1007/BF00994018.

Matteo Dalmasso, Marco Civera, Cecilia Surace, Valerio De Biagi, & Bernardino Chiaia, 2024. The seismic response and resilience of nearby underground infrastructures. https://doi.org/10.1201/9781003483755-183.

Dikmen, S.U., 2016. Response of Marmaray Submerged Tunnel during 2014 Northern Aegean Earthquake (Mw=6.9). *Soil Dynamics and Earthquake Engineering* 90, 15–31. https://doi.org/10.1016/j.soildyn.2016.08.006.

Dowding, C.H., Rozan, A., 1978. Damage to rock tunnels from earthquake shaking. *Ournal of the Geotechnical Engineering Division* 175–191.

Farrar, C.R., Worden, K., 2012. *Structural Health Monitoring*. Wiley. https://doi.org/10.1002/9781118443118.

Fedus, W., Rosca, M., Lakshminarayanan, B., Dai, A. M., Mohamed, S., & Goodfellow, I. (2017). *Many Paths to Equilibrium: GANs Do Not Need to Decrease a Divergence At Every Step*. http://arxiv.org/abs/1710.08446.

Goodfellow, I.J., Pouget-Abadie, J., Mirza, M., Xu, B., Warde-Farley, D., Ozair, S., Courville, A., Bengio, Y., 2014. *Generative Adversarial Networks*. http://arxiv.org/abs/1406.2661.

Haddadi, H., Shakal, A., Huang, M., & Parrish, J. (n.d.). *Report on Progress at the Center for Engineering Strong Motion Data (CESMD)*. www.strongmotioncenter.org.

He, Z., Li, W., Salehi, H., Zhang, H., Zhou, H., Jiao, P., 2022. Integrated structural health monitoring in bridge engineering. *Automation in Construction* 136, 104168. https://doi.org/10.1016/j.autcon.2022.104168.

Ho, T. (n.d.). *The design and construction of the New San Francisco-Oakland Bay Bridge (SFOBB) east span*.

Hwang, J.-H., Lu, C.-C., 2007. Seismic capacity assessment of old Sanyi railway tunnels. *Tunnelling and Underground Space Technology* 22 (4), 433–449. https://doi.org/10.1016/j.tust.2006.09.002.

Jiang, L., Zhong, J., Yuan, W., 2020. The pulse effect on the isolation device optimization of simply supported bridges in near-fault regions. *Structures* 27, 853–867. https://doi.org/10.1016/j.istruc.2020.06.034.

Lanzano, G., Bilotta, E., Russo, G., Silvestri, F., Madabhushi, S.P.G., 2012. Centrifuge Modeling of Seismic Loading on Tunnels in Sand. *Geotechnical Testing Journal* 35 (6), 104348. https://doi.org/10.1520/GTJ104348.

G. Lanzano, E. Bilotta, & G. Russo. (n.d.). Tunnels under seismic loading: a review of damage case histories and protection methods. *Publisher StreGa, Strategies for Reduction of the Seismic Risk*, 65–75.

Luleci, F., Catbas, F. N., & Avci, O., 2022. A literature review: Generative adversarial networks for civil structural health monitoring. In *Frontiers in Built Environment* (Vol. 8). Frontiers Media S.A. Doi: 10.3389/fbuil.2022.1027379.

Martucci, D., Civera, M., Surace, C., 2023. Bridge monitoring: Application of the extreme function theory for damage detection on the I-40 case study. *Engineering Structures* 279, 115573. https://doi.org/10.1016/j.engstruct.2022.115573.

Mccallen, D., Astaneh-Asl, A., Larsen, S., & Hutchings, L., 2005. *Dynamic Response of the Suspension Spans of the San Francisco-Oakland Bay Bridge*.

Michael Cabanatuan, C. S. W., 2004, April 17. *SAN FRANCISCO - OAKLAND / BART warns of possible leaks in Transbay Tube in big quake*.

Mirza, M., Osindero, S., 2014. *Conditional Generative Adversarial Nets*. http://arxiv.org/abs/1411.1784.

Nader, M., Manzanarez, R., & Maroney, B. (n.d.). *Seismic design strategy of the new east bay bridge suspension span*.

Nitschke, A. G., Mcrae, M., Associates, J., Francisco, S., & Ramirez, I. (n.d.). *NATM Excavation and Support Design and Construction of the Caldecott Fourth Bore*.

Okamoto, S., 1984. *Introduction to earthquake engineering*.

The Loma Prieta, California, Earthquake of October 17, 1989, Highway Systems. (n.d.). Doi: 10.1557-8.

Salimans, T., Goodfellow, I., Zaremba, W., Cheung, V., Radford, A., & Chen, X., n.d. *Improved Techniques for Training GANs*. https://github.com/openai/improved-gan.

Sarker, I. H., 2021. Deep Learning: A Comprehensive Overview on Techniques, Taxonomy, Applications and Research Directions. In *SN Computer Science* (Vol. 2, Issue 6). Springer. Doi: 10.1007/s42979-021-00815-1.

Sharma, S., Judd, W.R., 1991. Underground opening damage from earthquakes. *Engineering Geology* 30 (3–4), 263–276. https://doi.org/10.1016/0013-7952(91)90063-Q.

Thapa, B., Associates, J., Nitschke, A., Gall, Consultants, Z., Ramirez, I., Mcrae, M., & Gall, V., n.d. *Lessons learned from natm design and construction of the Caldecott fourth bore.*

Tsinidis, G., Rovithis, E., Pitilakis, K., Chazelas, J.L., 2016. Seismic response of box-type tunnels in soft soil: Experimental and numerical investigation. *Tunnelling and Underground Space Technology* 59, 199–214. https://doi.org/10.1016/j.tust.2016.07.008.

Tsinidis, G., de Silva, F., Anastasopoulos, I., Bilotta, E., Bobet, A., Hashash, Y.M.A., He, C., Kampas, G., Knappett, J., Madabhushi, G., Nikitas, N., Pitilakis, K., Silvestri, F., Viggiani, G., Fuentes, R., 2020. Seismic behaviour of tunnels: From experiments to analysis. *Tunnelling and Underground Space Technology* 99. https://doi.org/10.1016/j.tust.2020.103334.

Huibing Wang, Jinbo Xiong, Zhiqiang Yao, Mingwei Lin, & Jun Ren, 2017, July. Research Survey on Support Vector Machine. *People's Republic of China.*

Wang, W.L., Wang, T.T., Su, J.J., Lin, C.H., Seng, C.R., Huang, T.H., 2001. Assessment of damage in mountain tunnels due to the Taiwan Chi-Chi Earthquake. *Tunnelling and Underground Space Technology* 16 (3), 133–150. https://doi.org/10.1016/S0886-7798(01)00047-5.

Wold, S., Esbensen, K., Geladi, P., 1987. Principal component analysis. *Chemometrics and Intelligent Laboratory Systems* 2 (1–3), 37–52. https://doi.org/10.1016/0169-7439(87)80084-9.